

On the spectral density from instantons in quenched QCD

U. Sharan, M. Teper* (*UKQCD Collaboration*)

Theoretical Physics, University of Oxford, 1 Keble Road, Oxford, OX1 3NP, U.K.

Abstract

We investigate the contribution of instantons to the eigenvalue spectrum of the Dirac operator in quenched QCD. The instanton configurations that we use have been derived, elsewhere, from cooled SU(3) lattice gauge fields and, for comparison, we also analyse a random ‘gas’ of instantons. Using a set of simplifying approximations, we find a non-zero chiral condensate. However we also find that the spectral density diverges for small eigenvalues, so that the chiral condensate, at zero quark mass, diverges in quenched QCD. The degree of divergence decreases with the instanton density, so that it is negligible for the smallest number of cooling sweeps but becomes substantial for larger number of cools. We show that the spectral density scales, that finite volume corrections are small and we see evidence for the screening of topological charges. However we also find that the spectral density and chiral condensate vary rapidly with the number of cooling sweeps – unlike, for example, the topological susceptibility. Whether the problem lies with the cooling or with the identification of the topological charges is an open question. This problem needs to be resolved before one can determine how important is the divergence we have found for quenched QCD.

*ujji@thphys.ox.ac.uk, teper@thphys.ox.ac.uk

I. INTRODUCTION

There have been a number of recent lattice calculations that attempt to determine the instanton content of the vacuum in SU(2) [1] and SU(3) [2,3] gauge theories. One motivation has been to make contact with phenomenological instanton models [4,5]. Another aim has been to test certain long-held theoretical ideas, such as that instantons might play an important role in chiral symmetry breaking [4–6].

To identify the instanton content of fully fluctuating vacuum gauge fields (the latter obtained from lattice Monte Carlo simulations) is far from trivial. Indeed it is not entirely clear to what extent it is either meaningful or possible. Current techniques involve smoothening the lattice gauge fields on short distances and then using some pattern recognition algorithm to resolve the topological charge density into an ensemble of overlapping (anti)instantons of various sizes and positions. At present there is only some agreement between the results of the different approximate methods being used [2,3]. Thus all these calculations should be regarded as exploratory.

In this paper we shall focus on the calculations in [3]. There the smoothing of the rough gauge fields was achieved by a process called ‘cooling’ [7]. This is an iterative procedure just like the Monte Carlo itself except that the fields are locally deformed towards the minimum of the action (or some variation thereof). Although some quantities, such as the topological susceptibility, are insensitive to the amount of cooling (within reason) this is not the case for the number, size distribution and density of the topological charges. Whether this leads to a real ambiguity for physical observables is an important question. It might be that the ambiguity is only apparent and that fermionic observables calculated in these cooled instanton background fields do not show much variation with cooling. For example it might be the case that the instantons that disappear with cooling are highly overlapping $Q = \pm 1$ pairs which contribute no small modes to the Dirac operator. In that case the spectrum of small modes would be insensitive to cooling, and so would various fermionic observables such as the chiral condensate. How these physically important small modes actually depend

on cooling is the main question we address in this paper.

One might think that the reasonable way to approach all these questions would be to perform calculations directly on the cooled lattice fields using lattice versions of the Dirac operator. Although such explicit calculations do show that it is the instanton (would-be) zero modes that drive chiral symmetry breaking [8], one also finds that lattice artefacts spoil the mixing of the instanton near-zero modes [8] and this makes it difficult to draw reliable conclusions for the continuum limit. (Although very recent work with domain-wall fermions [9], and with related lattice fermions [10] suggests a promising avenue for progress.)

In this paper we shall calculate the interesting low lying eigenvalue spectrum of the Dirac operator by constructing an explicit matrix representation for a given background field of overlapping instantons and anti-instantons. Given our ignorance of the full structure of the vacuum, such a method is necessarily approximate. Our approach will be to simplify the details as much as possible while still incorporating both the important symmetries of the problem and (in the model calculations) the long-distance clustering properties of an ensemble of topological charges. Our expectation is that this should ensure that our answers are qualitatively reliable [11]. Some preliminary results using this method for configurations of instantons and anti-instantons distributed at random have been given elsewhere [12,13].

Let $\lambda_n[A]$ be an eigenvalue of the Dirac operator for some given gauge field configuration A : $i\mathcal{D}[A]\phi_n(x) = \lambda_n[A]\phi_n(x)$ defined in some space-time volume V . We know via the Atiyah-Singer Index theorem [14] that the eigenvalue spectrum will contain

$$Q[A] = n_- - n_+ \tag{1}$$

exact zero modes, where $Q[A]$ is the winding number of the gauge field configuration and n_{\pm} are the number of zero eigenmodes with positive/negative chirality. In the chiral limit a zero eigenvalue leads to a zero determinant; so gauge field configurations with non-trivial winding number are suppressed by the light quarks of full QCD. This suppression is lost in quenched QCD where the fermion determinant is set to unity. Let $\rho(\lambda; A) = \sum_n \delta(\lambda - \lambda_n[A])$ be the spectral density of the Dirac operator. One can relate the chiral condensate to the

spectral density via

$$\langle \bar{\psi}\psi \rangle = \lim_{m \rightarrow 0} i \int_0^\infty \frac{2m\bar{\nu}(\lambda, m)}{\lambda^2 + m^2}, \quad (2)$$

where $\bar{\nu}(\lambda, m) = \lim_{V \rightarrow \infty} \nu(\lambda, m)$ and $\nu(\lambda, m) = V^{-1} \langle \rho(\lambda) \rangle$. Care must be taken with the limits; if we reverse the order of the limits so that we take the chiral limit in a finite box then we will see symmetry restoration [8]. This is basically due to the fact that the eigenvalue spectrum has a gap of order V^{-1} when we deal with a system with a finite number of degrees of freedom (in our case the instantons). It is easy to see from equation (2) that the combination of the spectral gap and the absence of any exact zero modes in full QCD leads to symmetry restoration. This is however not the case in quenched QCD. In this case we still have the spectral gap but we also now have order \sqrt{V} exact zero modes, leading to $\lim_{m \rightarrow 0, V \text{ fixed}} \langle \bar{\psi}\psi \rangle \propto 1/m\sqrt{V}$. This pathological result is well known (see for example [8,12]) and is not the main thrust of the present paper. In this paper we concentrate on the contribution of the modes which are not Atiyah-Singer exact zero modes. It is these remaining modes which will contribute when the limits are taken as in equation (2). We will therefore ignore the contribution of the exact zero modes when calculating the chiral condensate. Another subtlety in equation (2) comes from the explicit quark mass dependence of the spectral density arising from the presence of the fermion determinant in the partition function. This quark mass dependence is absent in the quenched approximation; in this latter case one may safely evaluate the limits to get

$$\langle \bar{\psi}\psi \rangle = i\pi\bar{\nu}(0). \quad (3)$$

This is the Banks-Casher relation [15]. We immediately see that the low lying spectral density is crucial for this phenomenologically important condensate.

Equation (3) explains why instantons are a more interesting starting point for a discussion of chiral symmetry breaking than perturbation theory. If we neglect interactions then the perturbative vacuum becomes free. Here the Dirac eigenvalue spectrum grows as λ^3 . That is to say, the eigenvalues are far from zero. If on the other hand we neglect interactions amongst

(anti)instantons we get an exact zero-mode for each topological charge. This contributes a term $\propto \delta(\lambda)$ to $\overline{\nu}(\lambda)$. Introducing interactions will shift these distributions, but it is clear that if what one wants is a non-zero density of modes near $\lambda = 0$ then the latter approach is a more promising one than the former.

The above discussion suggests the following approach to calculating the contribution of topological fluctuations to fermionic observables such as the chiral condensate. First one decomposes the topological charge density of each gauge field into an ensemble of (overlapping) instantons and anti-instantons. One then constructs the space spanned by the would-be zero modes of these instantons. That is to say, for each instanton one finds the eigenfunction that would have zero eigenvalue if that instanton were isolated, and one constructs the space of linear combinations of these. Within that space one calculates the required physical observables such as the chiral condensate. This is most simply done by calculating the eigenvalues and eigenfunctions of the Dirac operator within this subspace.

This approach already represents an approximation. However to carry it out requires further approximations. Firstly one needs to identify the instantons in each gauge field. As remarked earlier we shall use the instanton ensembles obtained in [3]. To obtain these involved cooling (smoothing) the lattice gauge fields so as to reveal the topological charge density and then resolving this into overlapping (anti)instantons using some ‘pattern recognition algorithm’. The topological charge density rapidly changes as we cool a gauge field but one might reasonably hope that the physically important long distance fluctuations do not. For example, the total topological charge (the $p = 0$ projection of the charge density) is very stable under cooling, if the lattice spacing is small enough. Of course the total topological charge is a special quantity, and one of our main aims in this study will be to see how stable is the long distance fermionic physics under cooling. The second uncertainty involves the zero-modes. What we would like to use is a wave-function that corresponds to the zero mode of an isolated topological charge in the fully fluctuating vacuum. This is not known and in any case will not be unique. So we will employ some simple trial wavefunctions which have the basic property of being localised around the instanton. In addition we shall

neglect the detailed spinorial character of these wavefunctions except that we keep track of their chirality throughout the calculations. Clearly one can only believe those results of such a calculation that are insensitive to the particular form of the wave-function. In this paper our calculations will be performed using a hard-sphere wavefunction. Elsewhere [11] we have performed a detailed comparison with Gaussian wave-functions and with classical zero modes. The hard-sphere wave-function is particularly simple to work with in a periodic 4-volume, and produces Dirac spectra similar to the other trial wave-functions as long as the instanton gas is not too dilute. As we shall see below, the instanton ensembles that we take from [3] are typically very dense. The next approximation involves the calculation of the eigenvalues of the Dirac operator. This requires calculating the matrix elements of $i\mathcal{D}[A]$ within the space spanned by our zero modes for arbitrary fluctuating background gauge fields. Since we are not able to do this, we shall instead take the simplest possible approximation that embodies what we see as the most essential physics: we replace $i\mathcal{D}[A]$ by an operator which anticommutes with γ_5 (and thus only has non-zero matrix elements between states of opposite chirality), which has dimensions of inverse length as embodied by a factor of $1/l$ where l is a characteristic length scale of the states appearing in the matrix element, and which otherwise acts like a unit operator. This series of approximations retains those qualitative features of the full calculation that would seem to be the most critical, on the assumption that the qualitative physics should not depend on all the fine detail of the fluctuating gauge fields. It may turn out that this assumption is wrong and that an approach as simple as ours is not possible.

In the next section we introduce in detail our ‘toy’ model for calculating the contribution of an ensemble of topological charges to the spectral density. In the following section we apply this model to the ensembles generated in [3].

II. A TOY MODEL FOR EIGENVALUE SPLITTING

We consider the case of quenched QCD (i.e. the pure gauge theory). We construct a representation of the Dirac operator $i\mathcal{D}[A]$ for a gauge field A consisting of n_I instantons (I) and $n_{\bar{I}}$ anti-instantons (\bar{I}). Let each object have gauge field configuration A_i^\pm . We know that there are $|n_I - n_{\bar{I}}|$ exact zero modes, whose contribution to the spectral density we will ignore for the reasons discussed above. There are a further $n_I + n_{\bar{I}} - |Q|$ “would-be zero modes”; these are the modes which would be exact zero modes if the objects were non-interacting, as in the dilute gas approximation. In an interacting system these would-be zero modes become eigenvalues split symmetrically around zero. The splitting is symmetric as non-zero eigenvalues come in pairs $\pm\lambda$ due to the γ^5 symmetry $\{i\mathcal{D}, \gamma^5\} = 0$. It is these “would-be zero modes” which we expect to form that part of the low lying spectrum of the Dirac operator that is due to instantons, and so are of greatest importance in calculations of the chiral condensate.

A matrix representation is defined by $(i\mathcal{D}[A])|j\rangle = D_{kj}|k\rangle$ for some basis $\{|j\rangle\}$. It follows trivially that $D_{kj} = \langle k|i\mathcal{D}|j\rangle$ iff the basis is orthonormal. We choose our basis to be constructed out of the would-be zero modes coming from the individual objects $\{|\psi_1^+\rangle, \dots, |\psi_{n_{\bar{I}}}^+\rangle, |\psi_1^-\rangle, \dots, |\psi_{n_I}^-\rangle\}$ such that

$$i\mathcal{D}[A_i^\pm]|\psi_i^\pm\rangle = 0. \quad (4)$$

We are in effect writing the low lying eigenmodes of a given instanton configuration as a linear combination of the zero modes from the individual objects. If we were interested in the entire spectrum then we would have to include contributions from all modes but this is not necessary for our purpose. It is easy to see that

$$\begin{aligned} \langle \psi_i^+ | i\mathcal{D}[A] | \psi_j^+ \rangle &= 0 \\ \langle \psi_i^- | i\mathcal{D}[A] | \psi_j^- \rangle &= 0 \\ \langle \psi_i^+ | i\mathcal{D}[A] | \psi_j^- \rangle &\doteq V_{ij}. \end{aligned} \quad (5)$$

The first two identities follow from the γ^5 symmetry. Let us consider the third equation for a configuration consisting of a single $I-\bar{I}$ pair. The function V has, in principle, a dependence on the position of the centres of the objects (x_k^\pm), the sizes of the objects (ρ_k^\pm) and the relative colour orientation of the two objects. We choose to ignore the colour orientation for reasons of simplicity. We can also replace the covariant derivative $i\mathcal{D}[A]$ in the matrix element with $-i\partial$ using the equations of motion (4). So given a trial would-be zero mode wavefunction, we can actually calculate this matrix element as an overlap integral over some manifold (in all cases in this paper the manifold is simply the periodic box \mathbb{T}^4).

$$\begin{aligned}
V_{ij} &= \langle \psi_i^+ | i\mathcal{D}[A_i^+, A_j^-] | \psi_j^- \rangle \\
&= \langle \psi_i^+ | -i\partial | \psi_j^- \rangle \\
&= V(x_i^+, \rho_i^+, x_j^-, \rho_j^-).
\end{aligned} \tag{6}$$

Here we have assumed that the $I-\bar{I}$ gauge potential can be approximated as a sum of the individual I, \bar{I} gauge potentials (in some appropriate singular gauge). We note that (6) will be valid for an arbitrary number of (anti)instantons if their mutual separations are large. If however we are dealing with an arbitrary configuration consisting of more than a single $I-\bar{I}$ pair, then the function V is in general unknown. It will in fact have a dependence on all the objects within the configuration through the gauge field $[A]$. We also cannot replace the covariant derivative as before. We however choose to make this replacement anyway so that (6) holds for general configurations. Again, the main justification for doing so is simplicity.

In terms of this basis (and noting the above reservations), we can construct the $(n_I + n_{\bar{I}}) \times (n_I + n_{\bar{I}})$ matrix $D \equiv \langle \psi | i\mathcal{D} | \psi \rangle$ which has block zeroes on the diagonal and V, V^\dagger off block diagonal. There is however a fundamental objection to D being thought of as a matrix representation of the Dirac operator $i\mathcal{D}[A]$. This is due to the fact that the basis we have chosen is not orthonormal;

$$\begin{aligned}
\langle \psi_i^+ | \psi_j^+ \rangle &= U(x_i^+, \rho_i^+, x_j^+, \rho_j^+) \\
\langle \psi_i^- | \psi_j^- \rangle &= U(x_i^-, \rho_i^-, x_j^-, \rho_j^-)
\end{aligned}$$

$$\langle \psi_i^\pm | \psi_j^\mp \rangle = 0, \quad (7)$$

hence the matrix D is simply not a representation. (We have again ignored the possible dependence of the matrix element on the relative colour orientation of the objects; this is again for simplicity.) We can however construct an orthonormal basis $\{|\tilde{\psi}^+\rangle, |\tilde{\psi}^-\rangle\}$ using the standard Gram-Schmidt procedure,

$$\begin{aligned} |\psi_j^+\rangle &= R_{ij} |\tilde{\psi}_i^+\rangle \quad 1 \leq i \leq j \leq n_{\bar{I}} \\ |\psi_j^-\rangle &= S_{ij} |\tilde{\psi}_i^-\rangle \quad 1 \leq i \leq j \leq n_I. \end{aligned} \quad (8)$$

It is easy to see that in terms of this new orthonormal basis, a matrix representation of the Dirac operator is given by:

$$i\mathcal{D} \doteq \tilde{D} = \left(\begin{array}{cc} \overbrace{\langle \tilde{\psi}_i^+ | i\mathcal{D} | \tilde{\psi}_j^+ \rangle = 0}^{n_{\bar{I}}} & \overbrace{\langle \tilde{\psi}_i^+ | i\mathcal{D} | \tilde{\psi}_j^- \rangle = \tilde{V}_{ij}}^{n_I} \\ \langle \tilde{\psi}_i^- | i\mathcal{D} | \tilde{\psi}_j^+ \rangle = \tilde{V}_{ij}^\dagger & \langle \tilde{\psi}_i^- | i\mathcal{D} | \tilde{\psi}_j^- \rangle = 0 \end{array} \right) \left. \begin{array}{l} \} n_{\bar{I}} \\ \} n_I \end{array} \right\} \quad (9)$$

where

$$\tilde{V} = (R^{-1})^\dagger V S^{-1} \quad (10)$$

We see that this orthonormalization procedure preserves the chiral properties of the original wavefunctions; $\gamma^5 |\tilde{\psi}^\pm\rangle = \pm |\tilde{\psi}^\pm\rangle$. This matrix representation fulfills many of the requirements for the Dirac operator. It is easy to see that the elements of the matrices R, S and D are not random; they obey various triangle inequalities as they are given by overlap integrals between wavefunctions. Gram-Schmidt orthonormalization would be impossible for a general matrix without this property. It is also easy to see that \tilde{D} satisfies the γ^5 symmetry; all non-zero eigenvalues come in pairs $\pm\lambda$. Furthermore we see that the Atiyah-Singer theorem is obeyed; any configuration has at least $|n_I - n_{\bar{I}}|$ exact zero eigenvalues. If we consider the case of a single $I-\bar{I}$ pair (so orthonormalization becomes trivial), then it is easy to see that by choosing the function V appropriately, we can recover the correct eigenvalue splitting. (This is given by the overlap matrix element between would-be zero mode wavefunctions.)

All these features give us reason to believe that our toy model should capture the essential features of the mechanism whereby eigenvalues are split from zero.

All we have to decide is what form of trial would-be zero mode wavefunction to use for our objects. Simple examples include the hard sphere, Gaussian and classical zero mode wavefunctions. It is of course not possible to say which wavefunction will dominate the quantum vacuum. In this paper we concentrate on the simplest possible case, that of hard sphere wavefunctions;

$$\begin{aligned} \langle x | \psi_j^\pm \rangle &= 1 & |x - x_j^\pm| \leq \rho_j^\pm \\ &= 0 & \text{otherwise.} \end{aligned} \tag{11}$$

This choice would of course lead to an artificially singular form for V_{ij} and so (again in the interests of simplicity) we replace the derivative with $1/\sqrt{\rho_1\rho_2}$ so that both U and V are modeled by hard sphere wavefunctions but with the correct dimensions. We leave it to another publication to investigate more closely the universality of our results [11] for different wavefunction choices. In that study we perform extensive comparisons between hard-sphere, Gaussian and classical zero-mode wave functions, both on \mathbb{R}^4 and on \mathbb{T}^4 for a range of packing fractions and volumes. Although incomplete, this study shows that the qualitative features emphasised in the present paper are indeed universal. It is only these features, which are largely independent of the trial wavefunction used, that can be considered to be of significance and we can hope will survive in the full quenched QCD vacuum.

Each configuration in the ensemble consists of a set of positions, sizes and winding numbers (± 1) which label the objects in the vacuum. This set is either extracted from gauge field configurations generated by UKQCD [3] or alternatively, produced by a model that simply generates them at random. The advantage of the former method is that it may give a more accurate description of the topological content of the quenched QCD vacuum; the latter method has the advantage that we can obtain far higher statistics. And in some sense it isolates more cleanly the physics due to instantons, since the instantons in the lattice fields certainly contain correlations which are due to other dynamics. We use the method

outlined above to find the low lying eigenvalues for each given configuration. These are then used to generate the spectral density.

III. RESULTS

In [3] SU(3) lattice gauge field configurations of sizes $16^3 48$ at $\beta = 6.0$, $24^3 48$ at $\beta = 6.2$ and $32^3 64$ at $\beta = 6.4$ were cooled and the corresponding instanton ensembles extracted for various numbers of cooling sweeps. (We shall in the following frequently use “instantons” as a short-hand for “instantons and anti-instantons”.) Over this range of $\beta = 6/g^2$ the lattice spacing varies by a little less than a factor of 2 and these three volumes are approximately the same in physical units. Comparing the results at the three values of β enables the approach to the continuum limit to be studied. Of course, instantons can be large and it is important to control finite volume effects as well. For this purpose calculations were also performed at $\beta = 6.0$ on a much larger $32^3 64$ lattice. The conclusion was that finite volume corrections were negligible and that there was good scaling of, for example, the instanton size distribution, if one varied the number of cooling sweeps with β so as to keep the average number of instantons constant. (For an interesting recent analysis of the scaling properties, see [16].) Some properties of these lattice configurations are listed in Table I.

In this section we shall take these configurations, ranging in number from 20 to 100 depending on the lattice size and the value of β , and we calculate the spectral density of the would-be zero modes as described in the previous section. We shall, for simplicity, not employ some of the rather complicated procedures used in [3] for filtering out possible false instanton assignments. Rather we shall take the raw instanton ensembles from [3], corrected for the influence of the instantons upon each other but without applying any further filters. (Except that we throw away any charges that are larger than the volume available. This usually involves rejecting (much) less than 1% of the total number.) In addition, we calculate the size from the (corrected) peak height. We are confident that the results we obtain from these ensembles differ very little from the results we would have obtained using the slightly

different ensembles obtained by applying the more complex procedures of [3].

There are several questions we wish to address. These include:

- Do fermionic physical observables, such as the spectral density and the chiral condensate, exhibit a weak variation with cooling, implying that the rapid variation of the instanton ensemble that one observes is more apparent than real, or do they exhibit a strong variation?
- Do these fermionic physical observables also exhibit scaling and small finite volume corrections?

And more generally:

- Does a realistic ensemble of instantons break chiral symmetry spontaneously? Lattice calculations find that it does; but the presence of important lattice artefacts renders the conclusion suspect. Continuum calculations using model ensembles of instantons also find that they break chiral symmetry; but it is not clear that the real world is like the model.
- Is the spectral density of quenched QCD pathological? Some model calculations have found that the spectrum appears to diverges at $\lambda = 0$ [12,13,17]. Whether this is related to the appearance, within quenched chiral perturbation theory, of a logarithmic [17,18], or possibly power divergence [19], is also of interest.

Figure 1 shows the spectral density that results from the 50 configurations generated after 46 cooling sweeps on the $32^3 64$ lattice at $\beta = 6.0$. We see that the spectral density does not smoothly decrease to zero as $\lambda \rightarrow 0$, so the chiral symmetry will be spontaneously broken. However we also see a pronounced peak as $\lambda \rightarrow 0$, just like the divergence that characterises model instanton ensembles [12,13]. (Note that the exact zero modes contribute an invisible δ -function. Because this should be regarded as a finite volume effect, we shall not include it in the calculations of this section.) What is the functional form of this peak? We attempt to model the peak as a log divergence $\nu(\lambda) = a + b \ln(\lambda)$ and as a power divergence $\nu(\lambda) = a + b/\lambda^d$. Figures 2 and 3 show that both models fit the data well, an observation which is confirmed by the low chi-squared for the fit (see Table I). (The error estimates use the ‘jack-knife’ method and correlations between the errors in different eigenvalue bins are neglected. The observed scatter of values suggests that the latter should not be too bad an

approximation.) We should check that this result is not subject to large finite volume effects and to this end we compare the spectral density to that obtained from the $\beta = 6.0, 16^3 48$ lattice (a volume approximately ten times smaller). As shown in figure 4, whilst the result on the smaller volume is noisier, we find the densities are entirely similar, even down to the details of the forward peak. This shows that at least for these parameters any finite volume corrections are small. The chiral condensate as a function of quark mass is given in figure 5. We know that this order parameter must vanish for very small quark masses because of the gap in the eigenvalue spectrum (we cannot take the quark mass to zero in a finite box) and indeed it does. If we extrapolate to zero quark mass, whilst ignoring the finite volume dip at very small quark masses and the peak at small masses, we find that chiral symmetry is broken with an order parameter $\langle \bar{\psi}\psi \rangle^{\frac{1}{3}} \approx 400\text{MeV}$. Whilst this is larger than the phenomenological figure, $\langle \bar{\psi}\psi \rangle^{\frac{1}{3}} \sim 200\text{MeV}$, it is close considering the qualitative nature of our calculations. The fact it is larger is presumably a reflection of the high density of this gas of instantons.

Although the qualitative features of our spectrum do not require a specification of units, the comparison between different instanton ensembles does. The units we have chosen are as follows. Our length unit is chosen to be $32a$ at $\beta = 6.0$; so that the $32^3 64$ and $16^3 48$ lattices discussed in the previous paragraph have volumes 2 and 0.1875 respectively. We see from Table I that this corresponds to taking our length unit as $32a(\beta = 6.0) \simeq 32 \times 0.098\text{fm} = 3.136\text{fm}$. Thus our mass unit is the inverse of this, $\simeq 64\text{MeV}$. Since λ has dimensions $[m]^1$, this means that the eigenvalues shown in Figure 1 range from 0 to $\simeq 64\text{MeV}$: a reasonable range if what we are interested in is the spectrum $\lambda < \Lambda_{QCD}$. We maintain this unit throughout the calculations of this paper and we use the values of $a(\beta)$ listed in Table I to translate this unit to other values of β . Thus if we want to test for scaling all we need to do is to directly superpose the spectra as shown in our figures. (We shall do this later on in this section.)

We have focussed on the lattice calculations at $\beta = 6.0$ and after 46 cooling sweeps because it is only here that we can perform an explicit finite volume study. To go beyond

this constraint, and that imposed by the modest statistical accuracy of the lattice data, it is useful to analyse instanton configurations that have been generated in a simple toy model where the topological charges are placed at random positions in spacetime [11–13]. All these configurations are made to have zero topological charge since we know that $Q/V \rightarrow 0$ as $V \rightarrow \infty$, so we expect that taking only $Q = 0$ minimises finite volume corrections. A further simplification is that all charges in the random position model are the same size. By comparing this with the lattice data, where the instantons have various sizes, we will be able to investigate the effects of allowing the instanton sizes to vary. In figure 6 we plot a few of the spectral densities obtained from these ensembles of synthetic configurations. The different spectral densities are obtained by varying the packing fraction of the configurations (holding other parameters constant). The packing fraction is defined as the average number of topological charges multiplied by their average volume and divided by the total volume of spacetime, i.e. the quantity $\overline{N}_I \overline{V}_I / V$ in Table I. It is a measure of the fraction of the spacetime that would be occupied if the objects were non-overlapping: increasing the packing fraction whilst holding other variables constant increases the density of objects. We vary the packing fraction from 0.2 to 10 for high statistics ensembles (a minimum of 1266 configurations for the highest density to over 650000 configurations for the lowest). We observe a strong $\lambda \rightarrow 0$ divergence at low packing fractions which weakens as the density increases. As far as the functional form of this peak is concerned, Figure 7 and table II show that we can rule out the log divergence as a model for the peak for low density ensembles (packing fractions less than approximately 2). The power law divergence however gives a good fit for all densities (see figure 8 and table II). We note that it is only when we approach dense gases that the logarithmic fit to the divergence works equally well. Presumably this is simply a trivial consequence of the weakness of the power divergence, since

$$b\lambda^{-d} \simeq b - bd \ln(\lambda) \tag{12}$$

for small values of the exponent d . We plot a graph of the degree of divergence (the power d associated with the λ^{-d} divergence) versus the packing fraction in figure 9. This shows that

the divergence weakens as the packing fraction increases. It is not clear within our accuracy, whether there is a non-zero albeit very small divergence at very high densities, or whether the degree of divergence vanishes at some finite density. For practical purposes this question is not important; once the divergence is weak enough it will in any case have a negligible effect on the chiral physics in the vicinity of the physical quark masses. All this fits well with the naive picture whereby a higher packing fraction leads to greater overlaps (on average), leading to greater splitting of eigenvalues from zero, hence a weaker divergence (if any).

In figure 9 we also plot the degree of divergence corresponding to the $\beta = 6.0, 32^{364}$ lattice data. It would appear that the divergence is too large for the packing fraction; it lies approximately two sigma above the synthetic ensemble curve. It is therefore interesting to consider which particular aspect of the lattice data contributes to the divergence. The first possible factor is the non-trivial size distribution of the objects associated with the lattice data. We therefore set all objects in the lattice data to the same size (the mean $\bar{\rho}$ of the lattice ensemble). This reduces the packing fraction of the ensemble, since $\bar{\rho}^4 < \overline{\rho^4}$, and, as shown in figure 9, it also results in the degree of divergence fitting with that of the synthetic ensemble. The fact that a non-trivial instanton size distribution has a marked impact on the spectrum of small modes leads us to ask whether it is the small or the large instantons that drive this effect. To answer this question we systematically cull instantons of ever increasing size from the lattice instanton ensembles and see how this affects the spectral density. The results of this calculation are shown in figure 10. In this figure we show the densities obtained by only including objects with radii above a certain cut-off. We see that the peak is already significantly reduced if we exclude the $\sim 10\%$ of instantons with radii $\rho < 0.12$; and it is eliminated entirely if we exclude all instantons with $\rho < \bar{\rho} \simeq 0.18$. (If on the other hand we exclude the largest instantons, then we find that we strengthen the peaking at $\lambda = 0$.) This shows that the extra peaking we have observed with the lattice instanton ensembles is due to the smaller instantons. More generally, this demonstrates that it is possible to have small instantons driving a ‘divergent’ spectral density even in a high density gas. The reason for this unexpected phenomenon is actually quite simple. The large packing fraction of such

a gas is driven by the larger instantons (since the volume $\propto \rho^4$). The smaller instantons are rather dilute and are not likely to overlap significantly with each other. Instead they typically overlap completely with some of the much larger instantons. However this overlap is small: if we have a small instanton of radius ρ_s sitting on a large one of size ρ_l (of the opposite charge) then this will contribute $\propto \rho_s^4/\rho_s^2\rho_l^2 = (\rho_s/\rho_l)^2$ to the overlap matrix. The larger instantons, on the other hand, will have large overlaps with other large instantons (of the opposite charge) in addition to their small overlaps with small instantons. So they are less likely candidates for producing small eigenvalues. Thus the smaller instantons in an apparently dense gas can behave as a dilute gas with a corresponding peak at small eigenvalues. This would seem to be a phenomenon that might well be peculiar to quenched rather than full QCD.

It is also interesting to ask whether the non-random positioning of the instantons in the lattice ensembles makes a difference to the small- λ peak in the spectral density. We see from figure 9 and figure 11 that it does; positioning the objects at random (but incorporating other information such as the size distribution) increases the degree of divergence. Whilst there are systematic uncertainties (due to deciding which region of the data to fit the model to), this result is seen in all the lattice data that we have analysed. The simplest explanation for this is that we are seeing an effect of the topological charge screening that was observed in [3]. This tendency for opposite charges to ‘pair up’, will lead to an increased eigenvalue splitting and a weaker divergence. When we position the objects at random, this screening is lost and the degree of divergence is increased.

We return now to analyzing the lattice data and specifically to testing the effects of cooling. As a lattice field configuration is cooled, one finds [3] that the average size of the instantons increases and opposite charges annihilate. The former leads to fewer smaller objects whilst the latter leads simply to fewer objects in total per unit volume. Figure 12 shows the spectral density for the 20 configurations generated at $\beta = 6.4$ (corresponding to the smallest lattice spacing) on a $32^3 64$ lattice for 30, 50 and 80 cooling sweeps respectively. The configurations after 80 sweeps are thought to correspond to configurations after 23

sweeps at $\beta = 6.0$ (see [3] and figure 16). Hence all these configurations are denser than those analysed previously. We might therefore expect the peaking at $\lambda = 0$ to be weaker, or even non-existent. This is indeed what we see in figure 12. We also see something rather striking; as we cool more, and as we find fewer objects in the same volume, the entire spectral density shifts downwards in a way that is roughly proportional to the change in instanton number (see figure 13). This is in contradiction with the optimistic expectation that cooling, being a local smoothing, should have less effect at small eigenvalues (‘infrared physics’) and more effect at large eigenvalues (‘ultraviolet physics’) – as would occur if the main reason for the decrease of the number of charges with cooling was that heavily overlapping objects which produce large eigenvalues were annihilating. This naïve hope is seen to be unrealized. Cooling will also therefore alter the quark condensate, as we see in figure 14. (As usual this plot excludes the exact zero modes which would give a finite-volume peaking of the condensate at small quark masses.) Whilst we should not pay too much attention to the absolute normalisation of the quark condensate (given the qualitative nature of the calculation), our observation that cooling rapidly alters the quark condensate should be reliable. This creates an ambiguity that is particularly acute in the context of the small- λ divergence: depending on the amount of cooling, the instanton ensemble produces a divergence in quenched QCD that ranges from being very strong to being negligibly weak. The clear message is that these instanton ensembles differ strongly in the long-distance fermionic physics that they encode and that this is a problem that needs to be resolved before one can be confident that one understands the instanton content of the quenched QCD vacuum.

It would be nice to have a study of the large volume limit at $\beta = 6.4$, similar to the one at $\beta = 6.0$. Unfortunately that would require lattices much larger than $32^3 64$ and this is clearly impractical. By contrast, a nice feature of using our model is that it is easy to increase the volume and number of configurations and so test whether one has reached the infinite volume limit (and to obtain some idea of what a high statistics spectrum would look like). We show the results of such a calculation in figure 15. We compare the spectral

density generated from the instanton ensembles obtained after 80 cooling sweeps at $\beta = 6.4$ to that from high statistics synthetic ensembles with approximately half the volume and four times the volume respectively. The packing fraction has been chosen to equal that of the lattice ensemble. The lattice and model ensembles differ in that the latter contain objects of a single size positioned at random and with a total charge that is always zero, $Q = 0$. We observe however that the model spectra compare quite well with the lattice spectrum. One difference is that the lattice spectrum lacks a forward peak but this is in part due to the fact that the model ensemble always has $Q = 0$ while the lattice configurations do not. We note from the figure that the two volumes produce essentially identical (model) spectra. Thus the $V \rightarrow \infty$ limit appears to be under control.

Finally we address the question of scaling. In [3] it was shown that if we vary the number of cooling sweeps with β appropriately, then many properties of the instanton ensemble become independent of β once they are expressed in physical units. Is this also true of the more subtle features that are embodied in physical observables such as the chiral condensate? To investigate this we plot in figure 16 the spectral densities obtained after 23, 46 and 80 cooling sweeps on the $16^3 48$, $24^3 48$ and $32^3 64$ lattices at $\beta = 6.0, 6.2, 6.4$ respectively. These lattices have nearly equal volumes in physical units and the variation with β of the number of cooling sweeps is as prescribed in [3]. As we see the corresponding spectral densities are very similar showing that the important fermionic physical observables do indeed scale.

IV. CONCLUSIONS

In this paper we have investigated the implications of topology for the chiral condensate in quenched QCD. For the topological structure of the quenched QCD vacuum we have used the results of [3], where cooled lattice fields are decomposed into ensembles of instantons, and this is done for a variety of lattice spacings, space-time volumes and cooling sweeps. In addition, the lattice analysis has been supplemented by studying ensembles of instantons generated by a model that places them at random on the hypertorus. To calculate the

spectral density of the Dirac operator we have radically simplified the calculation keeping only the most essential symmetries and restricting the space of states to that spanned by the would-be zero modes of the topological charges. This means that while we may be able to address qualitative features, such as the variation of the spectral density with volume or with cooling, we would not expect more quantitative aspects, such as the actual value of the chiral condensate, to be accessible to our approach. (Although, as we have seen, it does not do too badly even for this.) In addition to the general features of the chiral condensate, a particular question we wished to address was whether such fermionic observables are insensitive to the cooling or not.

One qualitative feature that is common to all the instanton ensembles that we have investigated, is that they lead to spontaneous chiral symmetry breaking. A second, and striking, qualitative feature is that the spectral density diverges as $\lambda \rightarrow 0$ [12,17–19]. The divergence follows an approximate power law, $\propto \lambda^{-d}$, where d decreases as the density of the instantons increases. Moreover we have seen that it is possible to have a stronger divergence for denser gases if one has a sufficient range of instanton sizes, of the kind that one finds in the lattice instanton ensembles. We have also tried to fit the divergence with a logarithmic form, since this is what one expects in leading-order quenched chiral perturbation theory [18]. (It has also been seen by unfolding the microscopic spectral density obtained via Random Matrix Theory [17].) However such logarithmic fits are usually unacceptable, and where they are not it is a trivial consequence of the power exponent d being small, as in equation (12). It is interesting to note that if one attempts to sum the leading-logs of quenched chiral perturbation theory, one can obtain [19] a power divergence. The exponent of this divergence is $d = \delta/(1 + \delta)$ where the parameter δ is simply related to the elementary pseudoscalar flavour singlet annihilation diagram (whose iteration provides an estimate of the mass of the η' in full QCD). The strength of this diagram is related, in turn, to the topological structure of the quenched vacuum [20], and so this suggests an approach to constructing a detailed link between our approach and that of chiral perturbation theory. It is amusing to note that the most recent quenched QCD estimates [21] of δ , obtained from

chiral extrapolations where this parameter multiplies the quenched chiral log term, suggest a value $\delta \sim 0.1$ which is consistent with the kind of weak divergence we typically observe on the cooled instanton ensembles (see Table I). We intend to explore this link elsewhere [11].

We have furthermore found evidence, from a comparison of the Dirac spectral densities, for some of the claims in [3]: in particular for the screening of topological charges in the quenched QCD vacuum, for the smallness of finite volume corrections and for the claim that if the number of cooling sweeps is varied with β so that the number of topological charges per unit physical volume is constant, then the physical observables show scaling.

However we have also found that fermionic physical observables, such as the chiral condensate, vary strongly with the number of cooling sweeps. This contradicts the expectation that a moderate amount of cooling should only eliminate short distance fluctuations and so should not alter the physically important small- λ end of the spectral density. Whether this is a problem with cooling *per se* or whether, as one would expect, it indicates the increasing unreliability of the instanton “pattern recognition” algorithms of [3] as one decreases the number of cooling sweeps, is a question we are not able to address. The resulting uncertainty is particularly important for the significance of the small- λ divergence. We have seen that this divergence ranges from being strong to being negligible depending on which of the lattice instanton ensembles is used. It is strong for the larger number of cooling sweeps, which is where the instanton pattern recognition should be more reliable. On the other hand, a recent analysis [16] suggests that it is the instanton ensembles obtained with less cooling, where the low- λ peaking is negligible, that are the more physical. So although we do find that instantons generically produce a divergence in the chiral condensate of quenched QCD, it is not clear whether it is strong enough to have any impact on the predictions for physical quark masses. One lesson is unambiguous: there is more that needs to be done before one can claim to have completely understood the true instanton structure of the gauge theory vacuum.

ACKNOWLEDGEMENTS

The lattice instanton ensembles used in this work were produced by Douglas Smith and one of the present authors (MT). They were derived from gauge field configurations produced by UKQCD. We are grateful for this material. MT also wishes to acknowledge his debt to Nigel Dowrick without whose essential contributions, in an earlier collaboration, the present study would not have been possible. We are also grateful to various colleagues (including the referee) whose response to the first draft of this paper has helped to improve it. US wishes to thank PPARC for financial support (research studentship number 96314624). The computations herein were performed on our Departmental workstations. We are grateful to PPARC for support under PPARC grant GR/K55752.

REFERENCES

- [1] C. Michael and P. Spencer, Phys. Rev. D52 (1995) 4691;
Ph. de Forcrand, M. Garcia Perez and I-O Stamatescu, Nucl. Phys. B499 (1997) 409;
T. DeGrand, A. Hasenfratz and T. Kovacs, Nucl. Phys. B505 (1997) 417; B520 (1998) 301.
- [2] Ph. de Forcrand, M. Garcia Perez, J. Hetrick and I-O Stamatescu, hep-lat/9802017;
A. Hasenfratz and C. Nieter, hep-lat/9806026.
- [3] D.A Smith and M. Teper (UKQCD Collaboration), Phys.Rev. D58 (1998) 014505.
- [4] T. Schafer and E. Shuryak, Rev. Mod. Phys. 70 (1998) 323.
- [5] D. Diakonov, hep-ph/9602375, Varenna Lectures.
- [6] D. Caldi, Phys. Rev. Lett. 39 (1977) 121;
C. Callan, R. Dashen and D. Gross, Phys. Rev. D17 (1978) 2717;
R. Carlitz and D. Creamer, Ann. Phys. (N.Y.) 118 (1979) 429.
- [7] M. Teper, Newton Inst. NATO-ASI School Lectures, July 1997, hep-lat/9711011.
- [8] S.J. Hands and M. Teper, Nucl. Phys. B347 (1990) 819.
- [9] P. Chen et al, hep-lat/9811013; hep-lat/9811026; hep-lat/9812011.
- [10] R. Edwards, U. Heller and R. Narayanan, hep-lat/9811030;
H. Neuberger, Phys. Lett. B417 (1998) 141;
P. Niedermeyer, hep-lat/9810026.
- [11] U. Sharan and M. Teper, in preparation.
- [12] N. Dowrick and M. Teper, Nucl. Phys. (Proc. Suppl.) B42 (1995) 237.
- [13] U. Sharan and M. Teper, hep-lat/9808017.
- [14] M. Atiyah and I. Singer, Ann. Math. 87 (1968) 484.

- [15] T. Banks and A. Casher, Nucl. Phys. B169 (1980) 103.
- [16] A. Ringwald and F. Schrempp, hep-lat/9903039.
- [17] J. Verbaarschot and J. Osborn, Nucl. Phys. B525 (1998) 738.
J. Osborn, D. Toublan and J. Verbaarschot, hep-th/9806110.
J. Verbaarschot, private communication.
E. Shuryak, private communication.
- [18] S. Sharpe, Nucl. Phys. (Proc. Suppl.) B17 (1990) 146.
C. Bernard and M. Golterman, Nucl. Phys. (Proc. Suppl.) B26 (1992) 360.
M. Golterman, hep-ph/9710468.
- [19] S. Sharpe, hep-lat/9211005.
M. Golterman, private communication.
- [20] G. 't Hooft, Physics Reports 142 (1986) 357.
E. Witten, Nucl. Phys. B156 (1979) 269.
G. Veneziano, Nucl. Phys. B159 (1979) 213.
- [21] S. Aoki et al (CP-PACS Collaboration), hep-lat/9904012.
S. Sharpe, hep-lat/9811006.

TABLES

β	L^3T	a (fm)	Cools	N_c	\overline{N}_I/V (fm^{-4})	$\overline{N}_I\overline{V}_I/V$	d	χ^2/dof
6.0	16^348	0.098	23	100	9.1	4.2	-	-
6.0	16^348	0.098	46	100	3.2	1.9	-	-
6.0	32^364	0.098	46	50	3.5	2.84	0.251 ± 0.069	0.16
6.0 (<i>RP</i>)	32^364	0.098	46	50	3.5	2.84	0.585 ± 0.047	0.22
6.0 (<i>SS</i>)	32^364	0.098	46	50	3.5	1.85	0.186 ± 0.060	0.24
6.0 ($\rho > 0.12$)	32^364	0.098	46	50	3.1	2.82	-	-
6.2	24^348	0.072	46	100	8.9	4.9	-	-
6.4	32^364	0.0545	30	20	56.6	12.4	-	-
6.4	32^364	0.0545	50	20	21.7	8.5	-	-
6.4	32^364	0.0545	80	20	9.2	5.3	-	-

TABLE I. Some information about the data analysed in this paper. V is the total spacetime volume, \overline{V}_I is the average volume of an instanton in the ensemble, \overline{N}_I is the average number of topological charges per configuration and N_c is the number of configurations in the ensemble. *RP* stands for random positioning of objects whilst *SS* stands for all the objects being set to the same size. A degree of divergence d from a fit of the data to $\nu(\lambda) = a + b/\lambda^d$ is given wherever a fit with reasonable statistical and systematic errors is possible. χ^2/dof is the χ^2 per degree of freedom: the standard measure of goodness of fit.

f	$N_I + N_{\bar{I}}$	N_c	d	χ_p^2/dof	χ_l^2/dof
0.2	13 + 13	650000	0.656 ± 0.003	0.24	60
0.5	32 + 32	128000	0.695 ± 0.002	0.19	51
1.0	63 + 63	126000	0.595 ± 0.002	0.14	26
1.75	111 + 111	111000	0.309 ± 0.002	0.19	5
2.5	158 + 158	63200	0.075 ± 0.013	0.17	0.26
5.3	336 + 336	6720	0.013 ± 0.039	0.24	0.23
10.0	633 + 633	1266	0.009 ± 0.081	0.26	0.26

TABLE II. Some information about the synthetic ensembles analysed in this paper. f is the packing fraction in each configuration, $N_I + N_{\bar{I}}$ are the number of instantons and anti-instantons in each configuration respectively, N_c is the number of configurations in the ensemble, d is again the degree of divergence, and χ_p^2/dof is the standard chi-squared measure of goodness of fit for the power law fit, χ_l^2/dof is the chi-square for the log fit $\nu(\lambda) = a + b \ln(\lambda)$.

FIGURES

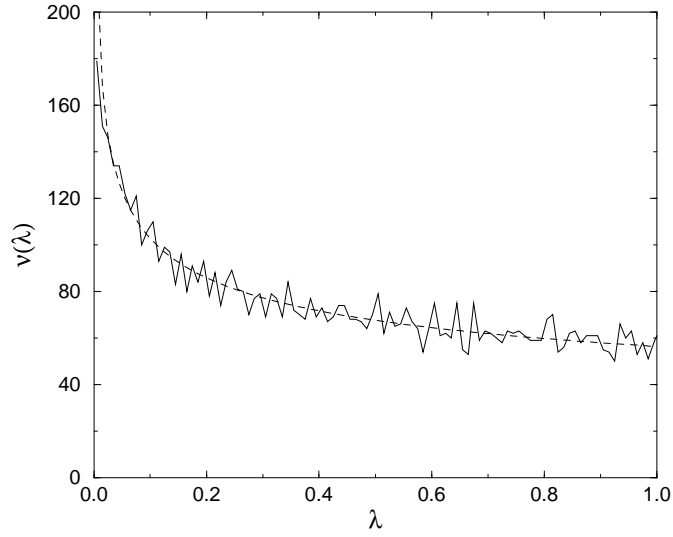


FIG. 1. The spectral density: $\beta = 6.0$, $32^3 64$, 50 configurations. Dashed curve is best power law fit $\nu(\lambda) = a + b/\lambda^d$.

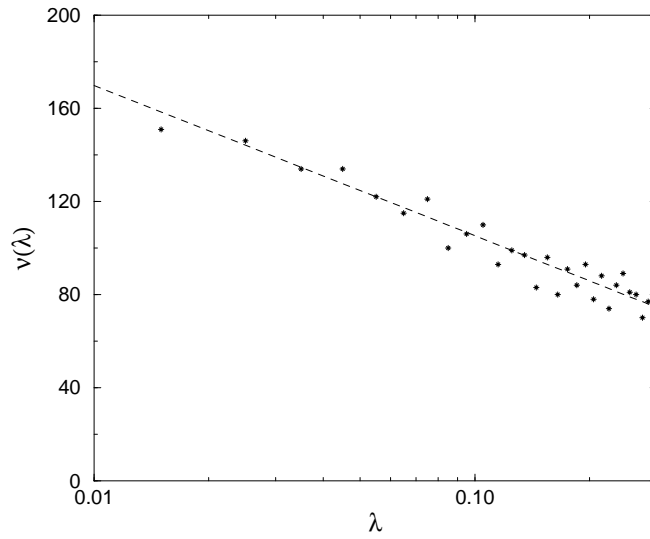


FIG. 2. The spectral density in figure 1, plotted on log-linear axes. Dashed curve is best log law fit $\nu(\lambda) = a + b \ln(\lambda)$.

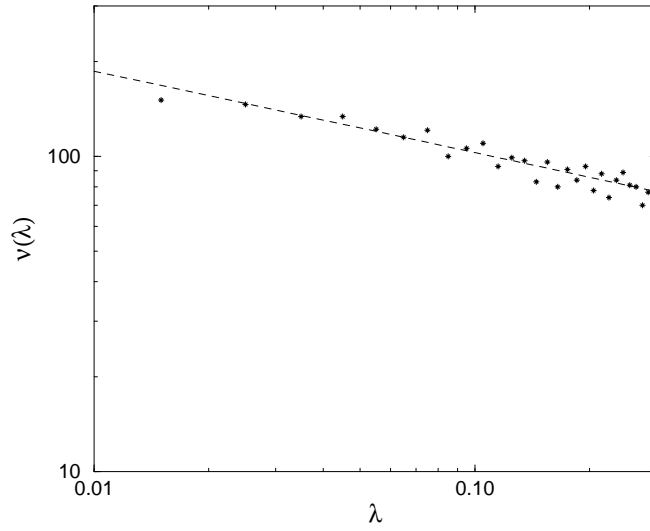


FIG. 3. The spectral density in figure 1, plotted on log-log axes. Dashed curve is best power law fit $\nu(\lambda) = a + b/\lambda^d$.

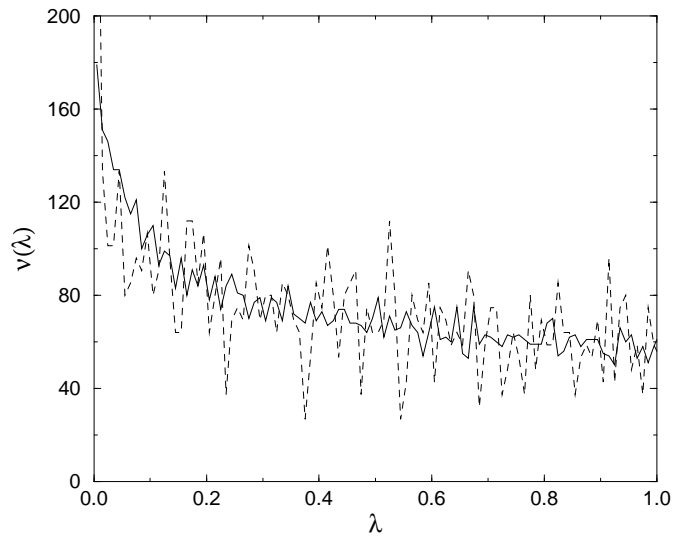


FIG. 4. Spectral densities from two different volumes at $\beta = 6.0$, after 46 cooling sweeps: $32^3 64$ (solid) and $16^3 48$ (dashed) lattices.

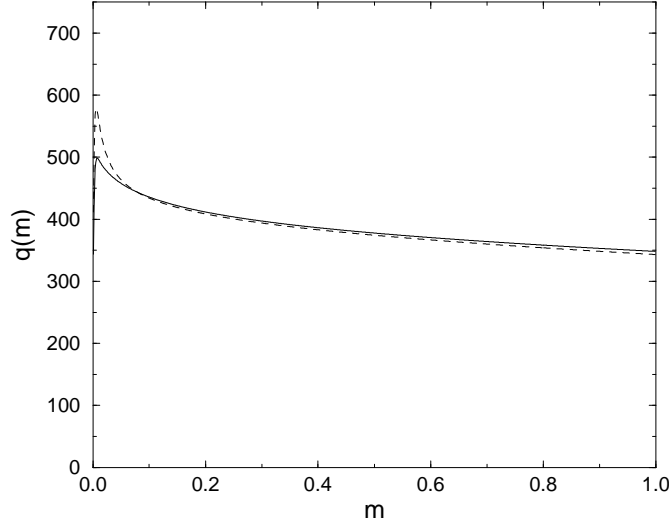


FIG. 5. $\langle \bar{\psi}\psi \rangle = (q(m)\text{MeV})^3$ as obtained from the $\beta = 6.0$ $32^3 64$ lattice data (solid), and from the $\beta = 6.0$ $16^3 48$ lattice data (dashed).

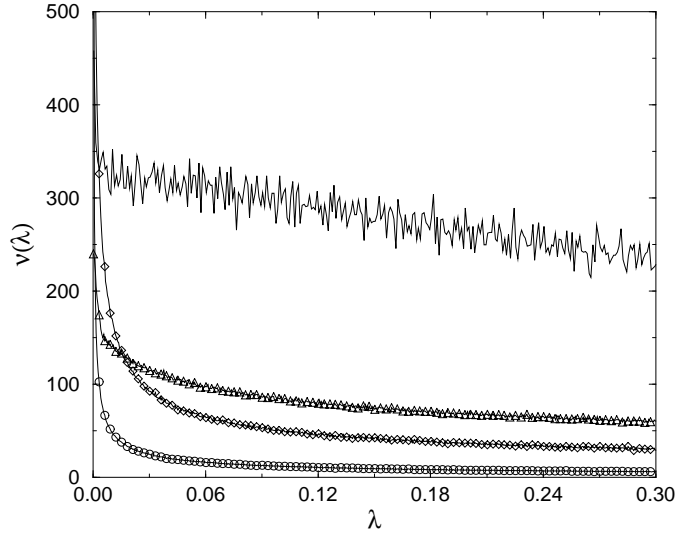


FIG. 6. Spectral densities from configurations generated by the random-position model, for various packing fractions, keeping the volume fixed and varying the number of charges as shown: $N\bar{V}_I/L^4 = 0.2$ (\circ $N = 13 + \overline{13}$), 1.0 (\diamond $N = 63 + \overline{63}$), 2.5 (\triangle $N = 153 + \overline{153}$) & 10.0 (solid $N = 633 + \overline{633}$).

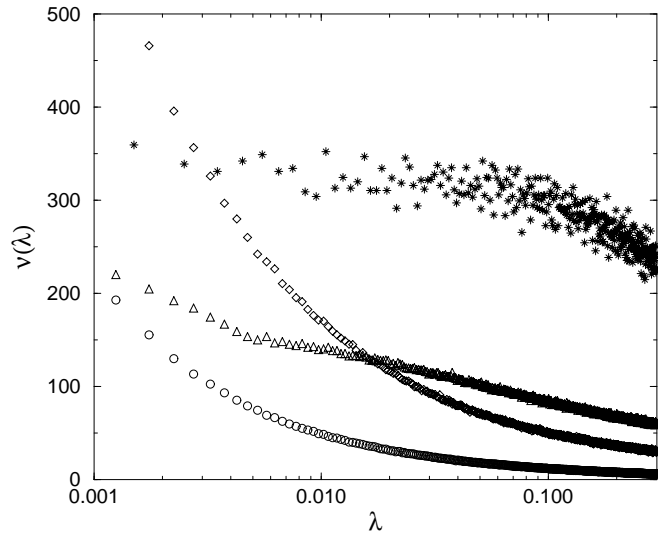


FIG. 7. Spectral densities in figure (6), plotted on log-linear axes.

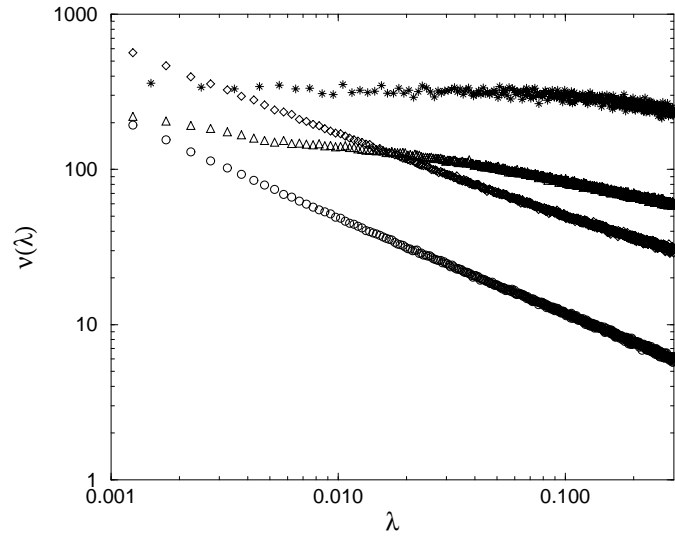


FIG. 8. Spectral densities in figure (6), plotted on log-log axes.

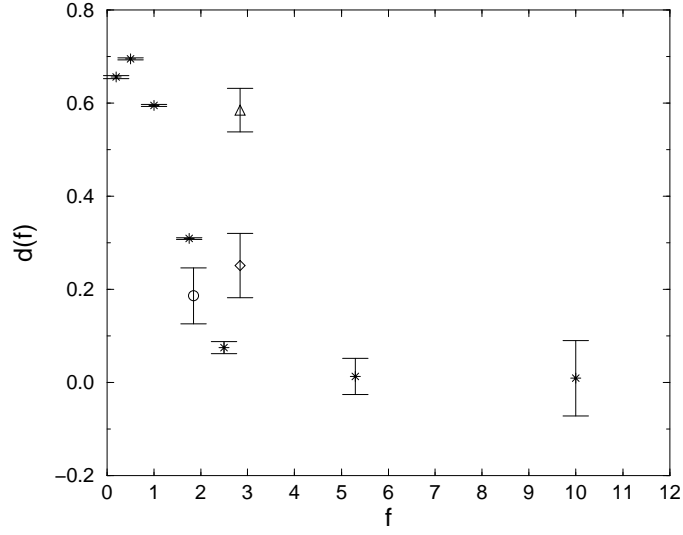


FIG. 9. Plot of power of divergence d as a function of packing fraction f . \star from random position model. \diamond from lattice data as in figure (1). \circ same, except all instantons of same size $\bar{\rho}$. \triangle as figure (1) except instantons positioned at random.

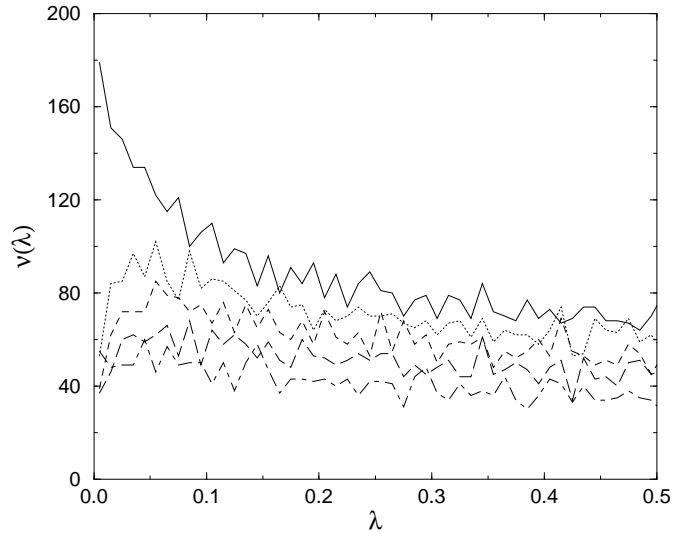


FIG. 10. Lattice Data: Solid line as figure (1). Dotted line only contains objects with $\rho > 0.12$, dashed line $\rho > 0.14$, long dashed $\rho > 0.16$, dot-dash $\rho > \bar{\rho} \approx 0.182$.

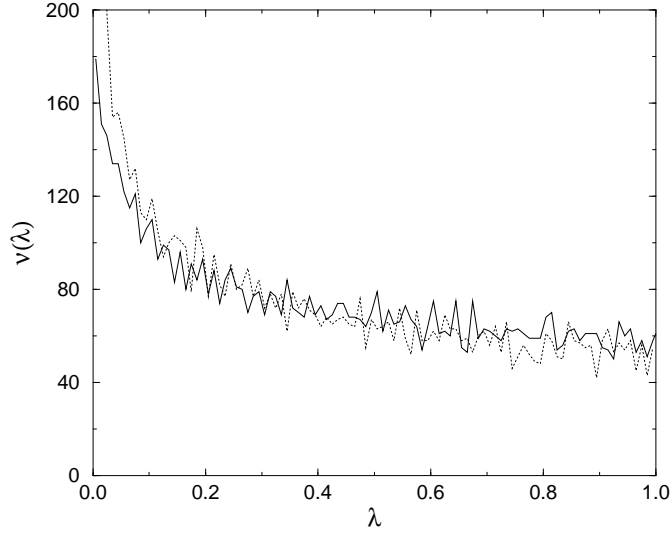


FIG. 11. The spectral density of figure 1 (solid), compared to the density obtained by positioning the same charges at random (dotted).

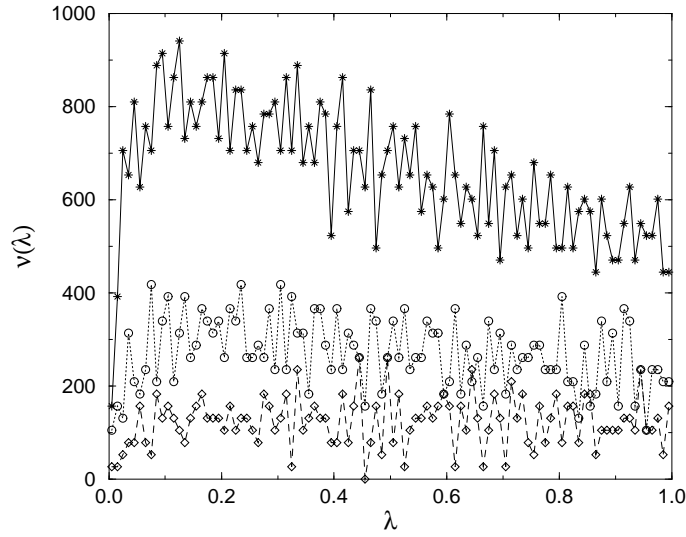


FIG. 12. The spectral densities obtained from the $\beta = 6.4$, $32^3 64$ configurations for various numbers of cooling sweeps: (\star) 30 cools, (\circ) 50 cools, (\diamond) 80 cools.

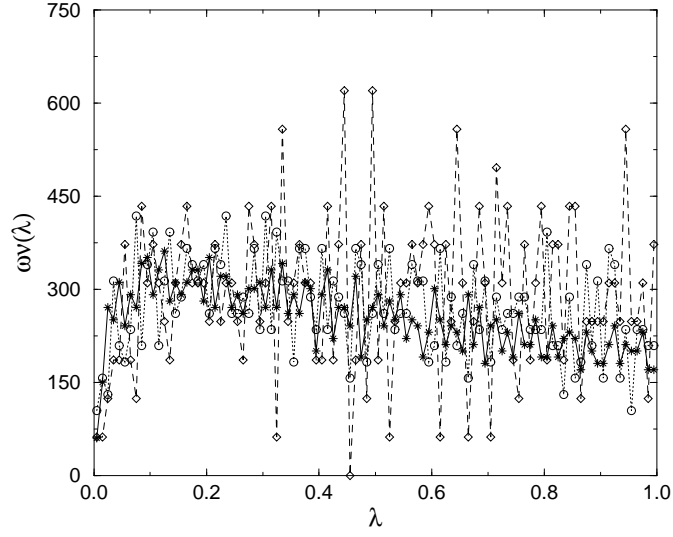


FIG. 13. The same densities as in figure 12 but rescaled by $\omega = n_{50}/n_i$, where n_i is number of topological charges after i cooling sweeps.

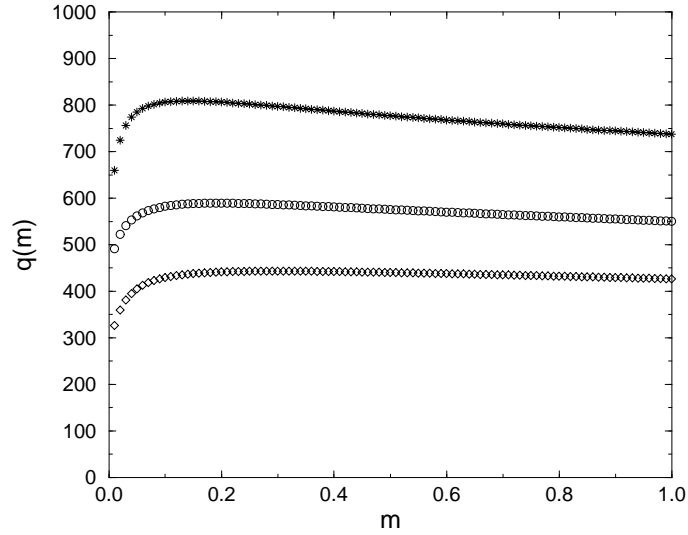


FIG. 14. $\langle \bar{\psi}\psi \rangle = (q(m)\text{MeV})^3$ obtained from the spectral densities in figure 12.

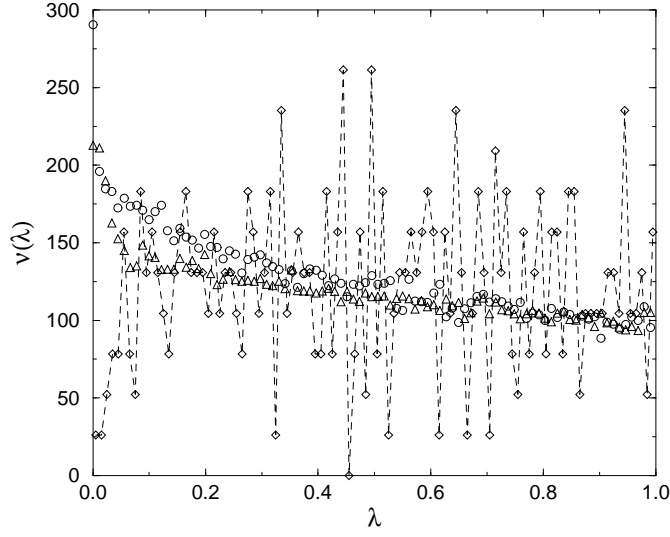


FIG. 15. Extending the calculations from actual lattice data. (\diamond) $\beta = 6.4$ $32^3 64$ data. (\circ), (\triangle) from synthetic ensembles with approximately four times the volume, and half the volume respectively.

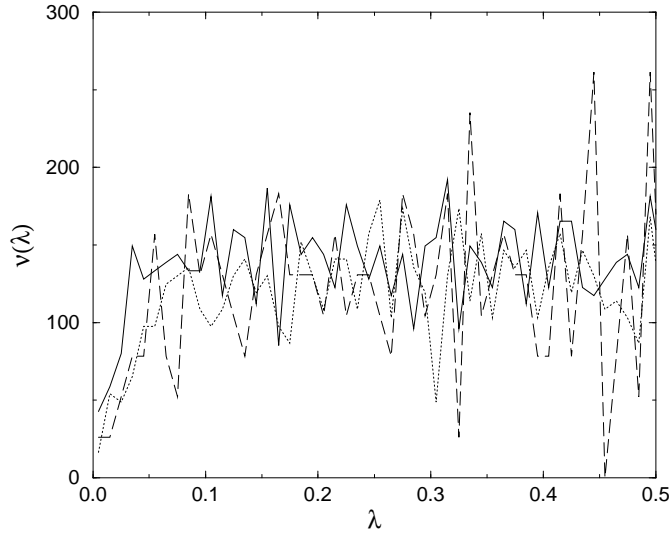


FIG. 16. The spectral densities obtained at $\beta = 6.0$, 6.2 , 6.4 after 23 (solid), 46 (dotted) and 80 (dashed) cooling sweeps respectively.